Geophysical Tomography in Engineering Geological Applications: A Mini-Review with Examples

Domenico Patella[*,1] and Sergio Maria Patella[2]

[1]*Department of Physical Sciences, University Federico II, Naples, Italy*

[2]*Via delle Alpi 16, Rome, Italy*

Abstract: An overview of the geophysical tomography interpretation method is presented. Two approaches are reviewed, (1) deterministic tomography inversion, developed for rock elasticity investigations, and (2) probability tomography imaging, developed in the domain of potential field methods. The theoretical basis of both approaches is initially outlined, then selected laboratory and field applications in different areas of engineering geology are presented and discussed. In particular, an ultrasonic laboratory experiment for the determination of the mechanical features of a block of marble and a crosshole seismic field experiment for quality assurance of a concrete placement are shown at first as examples of deterministic tomography inversion. Then, a geoelectrical field experiment aimed at detecting pollution leaks from a waste disposal and a self-potential field experiment for water flow modeling in a landslide are presented as examples of probability tomography imaging.

Keywords: Geophysical tomography, deterministic tomography inversion, probability tomography imaging, engineering and geological applications.

INTRODUCTION

Geophysical methods are widely applied to help solving many problems in engineering geology. The probability of a successful result increases if appropriate methods, based on the principles of information complementarity and coherency, are selected. Such a strategy is mostly advisable in delicate environments, where the adoption of absolutely non-invasive geophysical methods is the only possibility for target identification, prior to exploration.

Obtaining accurate geophysical models of buried targets has always been a difficult task, because of the mathematical difficulties and heavy calculations involved in the modeling. The newest hardware and software generations have been raised to such a high level of sophistication to allow for routine application of the interpretation tools developed over the past few years.

In the following sections a brief review of the principles of tomography in geophysics will be reported at first, focused on two main approaches, deterministic tomography (DT) inversion, developed for rock elasticity analyses, and probabilistic tomography (PT) imaging, proposed for geoelectrical field studies. The algorithms of both approaches are included to provide a rapid means for practical applications. Then, some examples of both approaches will be presented and discussed in order to show the performance level reached so far. In particular, an ultrasonic laboratory experiment for the determination of the mechanical features of a block of marble and a crosshole seismic field experiment for quality assurance of a concrete placement will be shown at first as examples of DT inversion. Then, a geoelectrical field experiment aimed at detecting pollution leaks from a waste disposal and a self-potential field experiment for water flow modeling in a landslide will be presented as examples of PT imaging.

This paper is a revised and expanded version of a previous paper [1].

DETERMINISTIC TOMOGRAPHY INVERSION

The DT inversion was developed in seismic prospecting in order to derive a detailed geometric model of the wave velocity pattern inside a medium, starting from the measured elastic wave traveltimes from sources to receivers [2-6]. This approach implicitly assumes the ray approximation, which is known to be strictly valid only for very high frequencies or equivalently for wavelength small compared with the size of the anomalies. Extensive experience has shown that the maximum permissible wavelength for the validity of the ray approximation must be not greater than one third of the anomaly size [7]. Otherwise, diffraction tomography and full waveform inversion must be adopted, as these try to make use of more of the information contained in the measured seismic waveforms. However, the serious problems involved with this process, because of the ambiguity in amplitude information [7], make the diffraction tomography of much less practical use, especially in engineering geology. Thus, we shall focus the attention only on traveltime tomography.

The relationship relating the wave traveltime t_i to the unknown slowness function $s(x,y,z)$ for a ray along the i-th path l_i of a set of M paths, is given by the Fermat integral

$$t_i = \int_{l_i} s(x,y,z)\mathrm{d}l \ , \ (i=1,2,..,M) \qquad (1)$$

In tomography inversion the delay time is introduced as the difference between the measured traveltime and the traveltime calculated in an a priori assigned reference model [3]. By dividing the excited volume into N elementary cells

*Address correspondence to this author at the Federico II University, I-80126, Naples, Italy; E-mail: patella@na.infn.it

1874-2629/09

(Fig. **1**), with the application of a perturbation technique it is possible to generate from the previous equation a system of linear equations, written in matrix form as

$$\delta \mathbf{t} = \mathbf{R} \cdot \delta \mathbf{s} \tag{2}$$

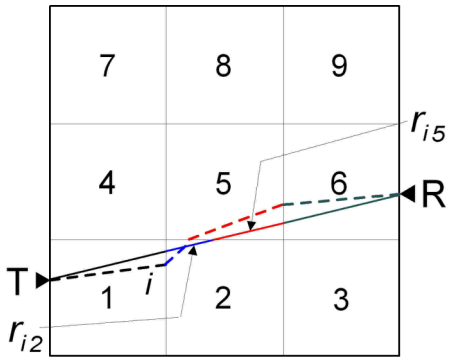

Fig. (1). A sketch of the approximations used for the application of the deterministic tomography inversion. The surveyed volume is approximated by a cubic array of elementary cells, characterized by different wave velocities. The full line connecting the transmitter T to the receiver R is the straight ray path approximating the unknown true ray path, represented by the sequence of dashed segments.

In this system, $\delta\mathbf{t}$ is a column matrix, whose element δt_i (i=1,..,M) represents the delay time along the i-th path, $\mathbf{R}$ is a rectangular sparse matrix, whose generic term r_{ij} (i=1,..,M; j=1,..,N) is the path length of the i-th ray in the j-th cell, and $\delta\mathbf{s}$ is a line matrix, whose generic element δs_j (j=1,..,N) is the slowness departure from the reference model in the j-th elementary cell.

When the experimental data space has dimensions much greater than those of the space of the unknowns (M»N), the above system becomes overdetermined, i.e. the number of rows of matrix $\mathbf{R}$ is greater than the number of columns. Hence, a least-squares approach must be applied by minimizing the Euclidean norm $\|\mathbf{R}\cdot\delta\mathbf{s}-\delta\mathbf{t}\|$. The solution for the vector $\delta\mathbf{s}$ is then given as

$$\delta\mathbf{s} = (\mathbf{R}^{\mathrm{T}}\mathbf{R})^{-1}\mathbf{R}^{\mathrm{T}}\delta\mathbf{t} = \mathbf{A}^{-1}\mathbf{R}^{\mathrm{T}}\delta\mathbf{t} \tag{3}$$

In solving this equation serious difficulties may be encountered, essentially related to the presence of small values within the matrix to be inverted. Therefore, in order to avoid singularities or near singularities, it is preferable to constrain the matrix $\mathbf{A}$ by introducing a damping factor β and use as solution for $\delta\mathbf{s}$ the damped equation [2,5]

$$\delta\mathbf{s} = (\mathbf{A} - \beta\mathbf{I})^{-1}\mathbf{R}^{\mathrm{T}}\delta\mathbf{t} \tag{4}$$

where $\mathbf{I}$ is the matrix of weights which is taken as unity.

The value to be assigned to β depends on the noise level in the data, in the sense that the higher is the noise the greater is β. It must be recalled that the damping factor β generally controls the number of iterations for convergence, not the final solution [2,5].

In order to raise the resolution power of the DT method, an iterative procedure can be applied, where the slowness model deduced from an inversion is used as the reference model for a new inversion. To start the iterative procedure an initial model must be assumed, which consists in assigning either a slowness distribution, if a priori information is available about the nature of the environment to be investigated, or, simply, a prefixed constant slowness, $s^{(0)}$. This constant value normally is the average slowness determined on the basis of the experimental data as follows

$$s^{(0)} = \frac{1}{M}\sum_{i=1}^{M}\frac{t_i^{(ex)}}{l_i} \tag{5}$$

where $t_i^{(ex)}$ is the experimental traveltime along the i-th ray path, l_i, which is approximated to a straight segment as in Fig. (**1**).

Accordingly, the corresponding reference traveltime along the i-th line is calculated as

$$t_i^{(0)} = s^{(0)}l_i = \left[\frac{1}{M}\sum_{i=1}^{M}\frac{t_i^{(ex)}}{l_i}\right]l_i \tag{6}$$

Thus, the initial slowness departure in the j-th elementary cell and delay time along the i-th path are respectively given as

$$\delta s_j^{(1)} = s_j^{(1)} - s^{(0)} \tag{7}$$

and

$$\delta t_i^{(1)} = t_i^{(ex)} - t_i^{(0)} \tag{8}$$

The slowness departures $\delta s_j^{(1)}$ (j=1,..,N) are unknown and must be determined putting the delay times $\delta t_i^{(1)}$ (i=1,..,M), estimated as above, into the above damped inversion system. Each path segment r_{ij} of the $\mathbf{R}$ matrix is given the length of the portion of the straightened i-th ray belonging to the j-th cell, like, *e.g.*, the r_{i2} and r_{i5} segments sketched in Fig. (**1**).

The solutions of the DT damped inversion system allow the initial estimates of the velocities $v_j^{(1)} = 1/s_j^{(1)}$ (j=1,..,N) to be obtained as

$$v_j^{(1)} = \frac{1}{\delta s_j^{(1)} + s^{(0)}} \tag{9}$$

Using these velocities as new starting model, which is, of course, no longer homogeneous, a new set of traveltimes can be calculated as follows

$$t_i^{(1)} = \sum_{j=1}^{N} s_j^{(1)} r_{ij} \tag{10}$$

from which the new delay times $\delta t_i^{(2)}$ (i=1,..,M) are calculated as

$$\delta t_i^{(2)} = t_i^{(ex)} - t_i^{(1)} \tag{11}$$

After putting this new set of delay times again into the DT damped inversion system, a new set of slowness departures $\delta s_j^{(2)}$ (j=1,..,N) is derived and, hence, new estimates of the velocities $v_j^{(2)} = 1/s_j^{(2)}$ (j=1,..,N) are obtained as

$$v_j^{(2)} = \frac{1}{\delta s_j^{(2)} + s_j^{(1)}} \tag{12}$$

Accordingly, for the k-th iteration the following sequence is realized

$$t_i^{(k-1)} = \sum_{j=1}^{N} s_j^{(k-1)} r_{ij} \rightarrow \delta t_i^{(k)} = t_i^{(ex)} - t_i^{(k-1)} \rightarrow$$

$$v_j^{(k)} = \frac{1}{\delta s_j^{(k)} + s_j^{(k-1)}} \tag{13}$$

The last iteration K will be that allowing the following condition to be satisfied

$$w_{K-1} - w_K \leq \Delta \tag{14}$$

where Δ is a pre-fixed discrepancy factor and w_k (k=1,..,K) is defined as the mean relative departure between the velocity values obtained from the k-th and (k–1)-th iterations, written as

$$w_k = \frac{1}{N} \sum_{j=1}^{N} \left| \frac{v_j^{(k)} - v_j^{(k-1)}}{\overline{v}^{(k)} - \overline{v}^{(k-1)}} \right| \tag{15}$$

where

$$\overline{v}^{(k)} = \frac{1}{N} \sum_{j=1}^{N} v_j^{(k)} \tag{16}$$

In the above derivation, in all of the iteration steps the ray paths have been assumed to be straight lines connecting sources and receivers. However, since the earth is not homogeneous, the rays in seismic transmission experiments bend significantly according to Fermat's principle or Snell's law. This fact should have, in principle, been taken into account in the above TD inversion algorithm. Thus, one should be aware that using the linear approximation with straight rays has important effects on the resolution of the reconstruction. Nevertheless, there are circumstances where using straight rays is recommended. First, if very high velocity contrasts are present, stable reconstruction with bent rays may be impossible while a straight ray reconstruction can still give useful information. Second, if the desired result is just a low resolution image showing whether or not an anomaly is present, then straight rays are entirely appropriate. Third, if bent rays are coupled with anisotropy, then straight rays are recommended too, since the nonuniqueness in the reconstruction for anisotropic wave appears so overwhelming that little can be done to overcome the problem [1].

PROBABILISTIC TOMOGRAPHY IMAGING

Differently from the previous DT approach, the purpose of the PT procedure is to retrieve an image of the spatial distribution of the occurrence probabilities of the sources of the observed anomalies [8-12].

Consider a datum surface S (Fig. **2**). Let $A(\mathbf{r})$ be the anomaly value at a datum point $\mathbf{r} \in S$, and assume that $A(\mathbf{r})$ can be discretized as a sum of partial effects due to Q elementary sources, viz,

$$A(\mathbf{r}) = \sum_{q=1}^{Q} a_q s(\mathbf{r} - \mathbf{r}_q) \tag{17}$$

The q-th elementary source, positioned at $\mathbf{r}_q$, is assigned a strength a_q and its effect at $\mathbf{r}$ is analytically described by the kernel $s(\mathbf{r}-\mathbf{r}_q)$.

The information power Λ over S associated with $A(\mathbf{r})$ is defined as

$$\Lambda = \iint_S [A(\mathbf{r})]^2 dS \tag{18}$$

which using the previous equation can be made explicit in the form

$$\Lambda = \sum_{q=1}^{Q} a_q \iint_S A(\mathbf{r}) \cdot s(\mathbf{r} - \mathbf{r}_q) \mathrm{d}S \tag{19}$$

Consider now a generic q-th addendum in this equation and apply Schwarz's inequality, thus obtaining

$$\left[\iint_S A(\mathbf{r}) \cdot s(\mathbf{r} - \mathbf{r}_q) \mathrm{d}S \right]^2$$

$$\leq \iint_S A^2(\mathbf{r}) \mathrm{d}S \cdot \iint_S s^2(\mathbf{r} - \mathbf{r}_q) \mathrm{d}S \tag{20}$$

Using the above inequality, it is possible to define a *source element occurrence probability* (SEOP) function as

$$\eta(\mathbf{r}_q) = C_q \iint_S A(\mathbf{r}) s(\mathbf{r} - \mathbf{r}_q) \mathrm{d}S \tag{21}$$

where

$$C_q = \left[\iint_S A^2(\mathbf{r}) \mathrm{d}S \iint_S s^2(\mathbf{r} - \mathbf{r}_q) \mathrm{d}S \right]^{-1/2} \tag{22}$$

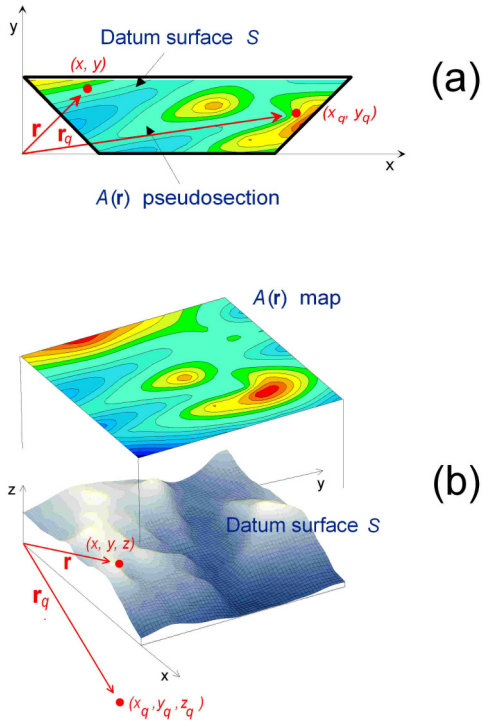

Fig. (2). A sketch view of the geometric assumptions for the application of the probability tomography imaging. The colored plot represents a typical geophysical anomaly field pseudosection (**a**) or map (**b**), obtained by a survey carried out along a straight profile (**a**) or on a non-flat ground surface (**b**). The vector **r** defines the generic datum point, whereas the vector $\mathbf{r}_q$ defines the generic unknown position of an elementary anomaly source pole.

The SEOP function satisfies the condition $-1 \leq \eta(\mathbf{r}_q) \leq +1$, and is interpreted as a measure of the probability of a source element with strength a_q placed at $\mathbf{r}_q$, being responsible of the observed anomaly field $A(\mathbf{r})$.

The PT procedure for a dataset collected over S consists in a scanning procedure based on the knowledge of the $s(\mathbf{r}-\mathbf{r}_q)$ space domain scanner function. It is a function depending on the technique used for sensing the earth and is mathematically well known, since it spatially describes the physical behavior of the field due to a source pole, which, according to the method used, can be an electrical charge [8, 9], a resistivity cell [10], an electrical current filament [11], or a gravitational point mass [12].

In practice, as the true source distribution responsible for a detected anomaly field $A(\mathbf{r})$ is unknown, a positive source pole of unitary strength is used to scan the surveyed space (the tomospace) and search where the real sources are most probably located. For any point $\mathbf{r}_q$, $\eta(\mathbf{r}_q)$ provides the occurrence probability of a positive ($\eta>0$) or negative source ($\eta<0$) located in that point, as responsible for the $A(\mathbf{r})$ field detected on the datum surface. By scanning the whole tomospace, a reconstruction of the source subsurface distribution can finally be imaged in a probabilistic sense, e.g. drawing a pile of horizontal slices at different depths, or a section across a single profile or also a sequence of parallel vertical sections across adjacent profiles.

The algorithm related to the PT imaging approach is now derived for the more general case of an $A(\mathbf{r})$ map, sketched in sector (**b**) of Fig. (**2**). The algorithm for the $A(\mathbf{r})$ pseudosection case, drawn in picture (**a**) of Fig. (**2**), will be derived as a particular case of the former one. It is worth recalling that the map is used to represent potential field data collected over areas, such as in the self-potential and gravity methods. The pseudosection, instead, is a typical plot used to represent, e.g., apparent resistivity and induced polarization data obtained by any electrode array moved along a straight profile.

In the first case, the projection of S onto the (x,y)-plane is assumed to be a rectangle $[0,X]\times[0,Y]$, which is discretized by a square grid using a step $\Delta\tau$ along both directions, and an $A(\mathbf{r})$ value is assigned at each node of the grid. If not measured, this value can be estimated by interpolation on the $A(\mathbf{r})$ survey map. Applying the normalization rule for surface integrals extended over irregular domains, and putting $x=\xi\Delta\tau$, $y=\gamma\Delta\tau$, $z=\zeta\Delta\tau$, $x_q=\xi_q\Delta\tau$,, $y_q=\gamma_q\Delta\tau$, $z_q=\zeta_q\Delta\tau$, $X=\xi_{max}\Delta\tau$, $Y=\gamma_{max}\Delta\tau$, with ξ, γ, ξ_q, γ_q, ζ_q, ξ_{max} and γ_{max} being integers, and the slopes along the x- and y-axis inside each square element of the grid as $\Delta z/\Delta x=\zeta_\xi$ and $\Delta z/\Delta y=\zeta_\gamma$, respectively, the SEOP function is discretized as follows

$$\eta(\xi_q,\gamma_q,\zeta_q) = C_q \sum_{\xi=0}^{\xi_{max}} \sum_{\gamma=0}^{\gamma_{max}} A(\xi,\gamma)$$

$$\times s(\xi-\xi_q,\gamma-\gamma_q,\zeta-\zeta_q)(1+\zeta_\xi^2+\zeta_\gamma^2)^{1/2} \quad (23)$$

where C_q is given by

$$C_q = \left[\sum_{\xi=0}^{\xi_{max}} \sum_{\gamma=0}^{\gamma_{max}} A^2(\xi,\gamma)(1+\zeta_\xi^2+\zeta_\gamma^2)^{1/2} \cdot \sum_{\xi=0}^{\xi_{max}} \sum_{\gamma=0}^{\gamma_{max}} \right.$$

$$\left. s^2(\xi-\xi_q,\gamma-\gamma_q,\zeta-\zeta_q)(1+\zeta_\xi^2+\zeta_\gamma^2)^{1/2} \right]^{-1/2} \quad (24)$$

For the second case, the algorithm is readily derived from the previous expressions as

$$\eta(\xi_q,\gamma_q) = C_q \sum_{\xi=0}^{\xi_{max}} \sum_{\gamma=0}^{\gamma_{max}} A(\xi,\gamma)$$

$$\times s(\xi-\xi_q,\gamma-\gamma_q,\zeta-\zeta_q) \quad (25)$$

with

$$C_q = \left[\sum_{\xi=0}^{\xi_{max}} \sum_{\gamma=0}^{\gamma_{max}} A^2(\xi,\gamma) \right.$$

$$\left. \cdot \sum_{\xi=0}^{\xi_{max}} \sum_{\gamma=0}^{\gamma_{max}} s^2(\xi-\xi_q,\gamma-\gamma_q,\zeta-\zeta_q) \right]^{-1/2} \quad (26)$$

APPLICATIONS

An Ultrasonic DT Laboratory Experiment

Seismic tomography is one of the most powerful tools for the investigation of the mechanical features of rock masses [13]. The technical developments during the past ten years have provided a low cost means of acquisition and processing of large amounts of data. The use of the DT methods has thus dramatically increased in engineering geology. Current applications are foundation surveying, rock qualification for waste disposal, cave detection, fracture and fault location and rock asperities, using different types of seismic waves, namely P, S, Love and Rayleigh waves [14].

Furthermore, there is a large interest in the properties of naturally consolidated soils and rocks, which stems from the relevance that these materials have in building and dredging industry. Since soils and rocks are both compositionally and behaviorally complex, there is a need to characterize their geomechanical properties in laboratory. One such example performed at the University Federico II of Naples is presented below [1].

Fig. (**3**) shows a sketched plane view of a (32×32×6) cm^3 composite block, consisting of a nearly (11×16×5) cm^3 piece of marble with v_p=4600 m/s, encased within a chalky matrix (v_p=1600 m/s). A Panametrics 5058PR ultrasonic impulse generator and two Panametrics X1021 P-wave transducers with a resonance central frequency of 50 kHz, coupled with a Tektronix TDS430A digital oscilloscope, were used.

The block was virtually subdivided into 64 equal cells of volume (4×4×6) cm^3. The measurement procedure consisted each time in fixing the transmitter and receiver pair at the centre of the vertical facelets of area (4×6) cm^2, lying along the opposite faces of the encasing block, and moving one or both transducers at the constant step of 4 cm, as shown in Fig. (**3**). In order to improve resolution, the transmitter and receiver roles were interchanged, thus obtaining a total of M=256 ray paths.

The results which were obtained from the application of the DT algorithm are shown in the 2D map of Fig. (**4**). An initial damping factor β=0.1 and a discrepancy factor Δ=1 were assumed [2-6]. A clear conformity appears between the irregular form of the piece of marble and its reconstructed physical model. This picture, jointly with the reasonable es-

timate of the velocity profile, demonstrates how high the resolution is of the DT technique in laboratory.

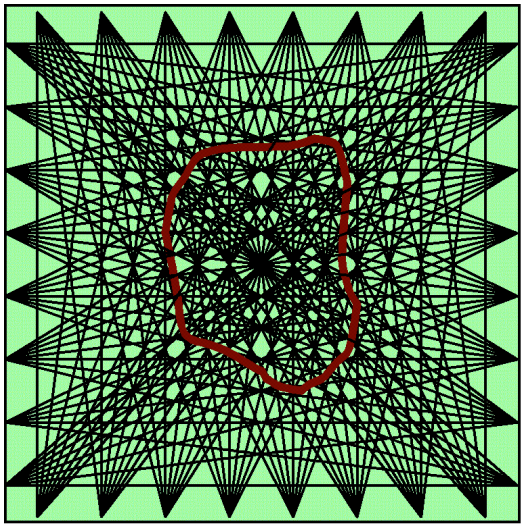

Fig. (3). Laboratory application of the deterministic tomography inversion method to an experiment of ultrasonic wave transmission across a block of marble [1]. The sample boundary is contoured in red. The dense mesh of black lines represents the ray path geometry generated by the regular transducer-receiver layout at the periphery of the encasing block.

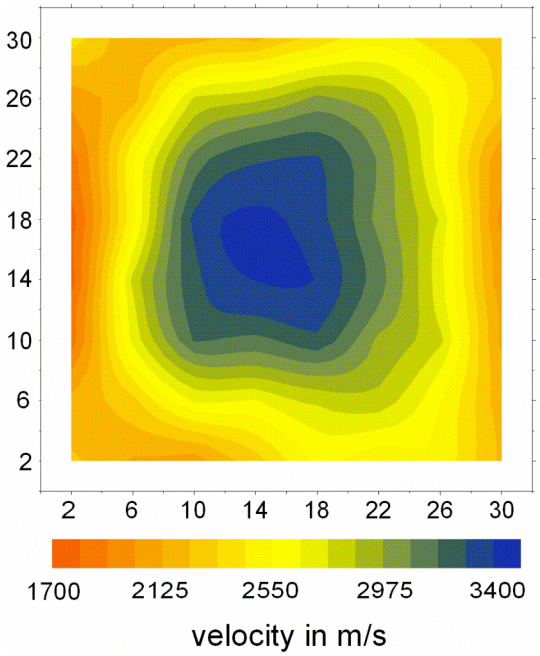

Fig. (4) The velocity model results from an experiment of ultrasonic wave transmission across the block of marble depicted in Fig. (**3**) [1].

A Crosshole Seismic DT Field Experiment

Crosshole seismic prospecting, where both sources and receivers are positioned within subsurface boreholes, has become a well established technique in civil engineering site investigation over the past 25 years [13]. It is currently applied also in the petroleum industry especially associated with producing problems [14]. The interest is undoubtedly due to the fact that it is possible to determine vital geotechnical features, in situ, from either first arrivals or the entire wavefield at the receiver borehole, without the need to drill additional expensive boreholes and transport samples to a distant laboratory. Surveys can also be carried out where site accessibility is too restricted for conventional surface geophysics, as e.g. in urban areas, and can be used to verify inter-borehole interpretation.

Crosshole DT is usually classified into three categories: (1) velocity DT, where the traveltime of the first arrival of the seismic impulse is measured in the interwell space; (2) attenuation DT, where the interest is on the amplitude of the first arrivals, with the objective of measuring absorption of seismic energy between boreholes; (3) elastic DT, where the entire wavefield is processed, with the scattered wavefield providing additional information.

Technique (1) is the quickest approach in current field practice. The first step in a prospecting consists in measuring the first-arriva1 traveltimes between sources and receivers located in two boreholes (Fig. **5**). By combining traveltimes from a number of sources and receivers at different depths in the two holes, one can estimate the P-wave velocity distribution on a 2D section, using a DT numerical algorithm as previously explained.

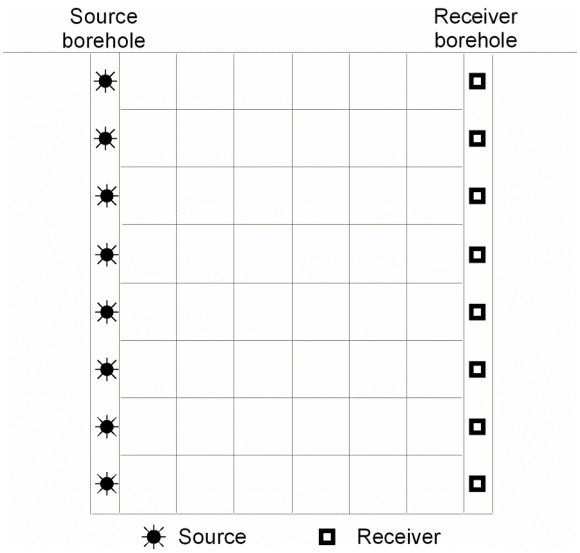

Fig. (5). A sketch of the source-receiver configuration for crosshole seismic tomography.

Crosshole DT has also come into widespread utilization for quality assurance of concrete placement in concrete drilled shaft foundations, particularly when they are drilled using wet-hole drilling methods, due to the risk of concrete contamination. The velocity of sound between water-filled cast-in-place access tubes is measured. The velocity of the sound wave traveling from source to receiver in a horizontal plane determines the presence of anomalous regions (due to water or air-filled voids or soil intrusions) and therefore the quality of the concrete.

An experiment is now illustrated, taken from a project performed at the University of Massachusetts, Amherst, to non-destructively model known foundation defects for 6 drilled shafts [15].

2D tomography data were collected for all tube pairs. A sample tomogram for the tube pair 1-2 quantifying defects between −2.2 m and −3.3 m is presented in Fig. (**6**). The ab-

solute velocity scale shows color assignments and was designed to most clearly depict the anomaly. The defect is successfully imaged and appears to be characterized by velocities dropping to nearly 2.4 km/s, thus indicating its severity. The defect was a 30 cm diameter plastic bucket combined with a fiberglass insulation [15].

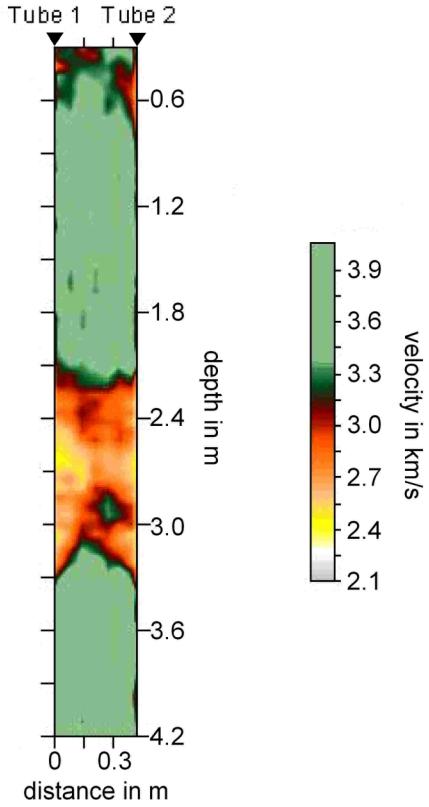

Fig. (6). Crosshole tomography elaborated from a 2D dataset collected between two tubes during an experiment aimed at detecting defects in concrete drilled shaft foundations (redrawn after [15]).

A Geoelectrical PT Field Experiment

The geoelectrical survey method is often used to obtain resistivity information near and over waste disposal sites. It helps mapping both vertical and horizontal distributions of contamination caused by increase of solutes in groundwater relative to background levels, which is reflected in increase of the electrical conductivity of the water bearing rock [16].

Dipole-dipole profiling is the most adopted technique, as it provides high vertical and lateral sensitivity. The so-called apparent resistivity pseudosection representation allows a preliminary inspection of the anomalies to be made.

Figs. (**7**, **8**) refer to a field survey performed on a waste disposal site in southern Italy [1]. The survey site consists of a waterproofed basin dug out in a sandy-clayey terrain down to 17 m depth below ground level. The basin was completely filled with waste and leaks of pollutant were suspected across tears in the 5 mm thick impermeable sheets.

The pseudosection in Fig. (**7**) shows apparent resistivity variations in the range 0.8-10 Ωm. The highest apparent resistivities were only marginally detected along the top part of the pseudosection, whereas below, since a few m of pseudodepth, very low values of about 1 Ωm are met with the presence of small nuclei including even lower values.

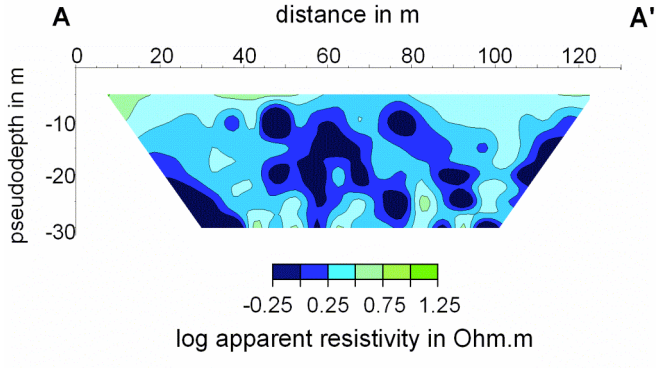

Fig. (7). Example of application of the probability tomography method to a geoelectrical dipole-dipole dataset collected along a profile over a waste deposit [1]. The dipole-dipole pseudosection for a preliminary assessment of the anomaly pattern.

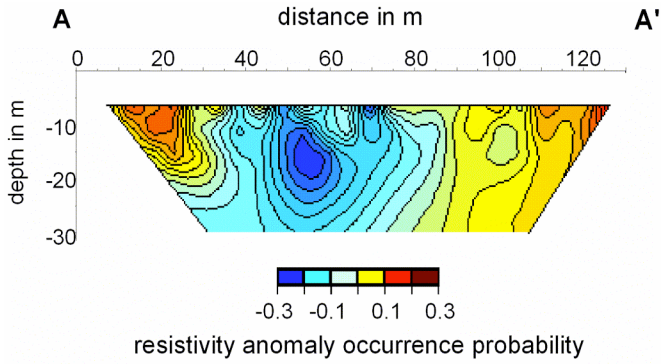

Fig. (8). Probability tomography 2D imaged section obtained from the pseudosection reported in Fig. (**7**).

Fig. (**8**) shows the results of the PT algorithm applied to the pseudosection of Fig. (**7**). The SEOP function represents, in the geoelectrical case, the resistivity anomaly occurrence probability function [10]. The most remarkable feature is now the presence of the lowest negative values of the SEOP function at the left-hand border of the central part of the section. In particular, the large negative SEOP nucleus, located between 40 m and 60 m along the horizontal distance scale, appears to propagate beyond the 17 m depth of the impermeable sheet. The conclusion is thus that the pollutant solutes may have overstepped the barrier, although its diffusion appears to be limited to a short distance due to the low permeability of the sandy-clayey hosting deposit.

A Self-Potential PT Field Experiment

The self-potential (SP) method is gaining increasing importance in landslide modeling and monitoring, because of its sensitivity to underground water flows. In fact, the circulation of more or less ionized fluids in porous media may induce electrical spontaneous polarization, which generates on its turn an electrical field easily measurable at surface.

From the theoretical point of view, the SP method is founded on the coupled flows general theory. In restricted areas and at shallow depths, in the absence of impressed external electric fields and assuming both dissolved salt

concentration and temperature gradients generally negligible, the streaming potential formula $\nabla U=(\varepsilon\zeta/\eta\sigma)\nabla P$ is valid, where ε, η and σ are the dielectric constant, viscosity and conductivity of the fluid, respectively, and ζ is the so-called zeta-potential. The leading parameter ζ is negative in the most recurrent cases of clayey, silty, marly, muddy and sandy sliding terrains [8,17].

Figs. (**9**, **10**) refer to a field survey performed on a sliding slope in a small village of Central Italy, seriously affecting the stability of some houses [18]. In particular, Fig. (**9**) shows the SP map obtained in the survey area using two different representations.

Two different patterns can be easily distinguished in this map. The first pattern is characterized by a low wavenumber field, which is the typical surface response of a deep bipolar source. It spreads over the whole surveyed area. Accounting for the previously reported streaming potential relationship, and knowing that the landslide mass is made of a mixture of clayey and silty terrains, this pattern allows the existence of a water flow to be hypothesized in the basal portion of the landslide, downhill along the longitudinal direction of the surveyed rectangle.

The second, more complex pattern is characterized by the superposition of higher wavenumber fields, associated with a set of shallower bipolar sources. The main feature of this pattern is the presence of two trends, one longitudinal and the other transversal. Although the depth of these shallower sources cannot be established at this stage, the two trends allow the existence of two hypothesized fissured striking bands, inside which a sub-vertical fluid circulation should reasonably occur.

We consider now the main features emerging from the SP PT images at different depths, reported in Fig. (**10**). For the SP method, the meaning of the SEOP function is the probability of an electrical charge occurrence, given that the observed SP map is nothing but the surface evidence of a more or less complex polarization state of electrical charges underground [8]. Firstly, it can be argued that the boundary separating the shallow bipolar source zone from the deep bipolar source zone may be positioned at around −15 m of depth. Moreover, starting from the shallowest PT image at −2.5 m down to that at −10 m, one can observe that the SEOP minimum values for the location of the negative poles are found at depths not greater than −2.5 m, whereas the SEOP maximum values for the location of the positive poles are met in the depth range from −5 m to −10 m. The evidence that the positive poles appear deeper than the negative poles would mean that the water moves downward, as it is expected during a rainy period, like in the winter season when the dataset was acquired.

CONCLUDING REMARKS

An overview of the geophysical tomography procedure for engineering geological applications has been presented. The two approaches of the deterministic tomography (DT) inversion, developed for acoustic velocity analysis in rocks, and the probability tomography (PT) imaging, proposed for the study of the electric properties of the subsoil, have been outlined. The theoretical principles of both approaches have been reported and four case-studies have been discussed to demonstrate the resolution power reached by tomography in geophysics.

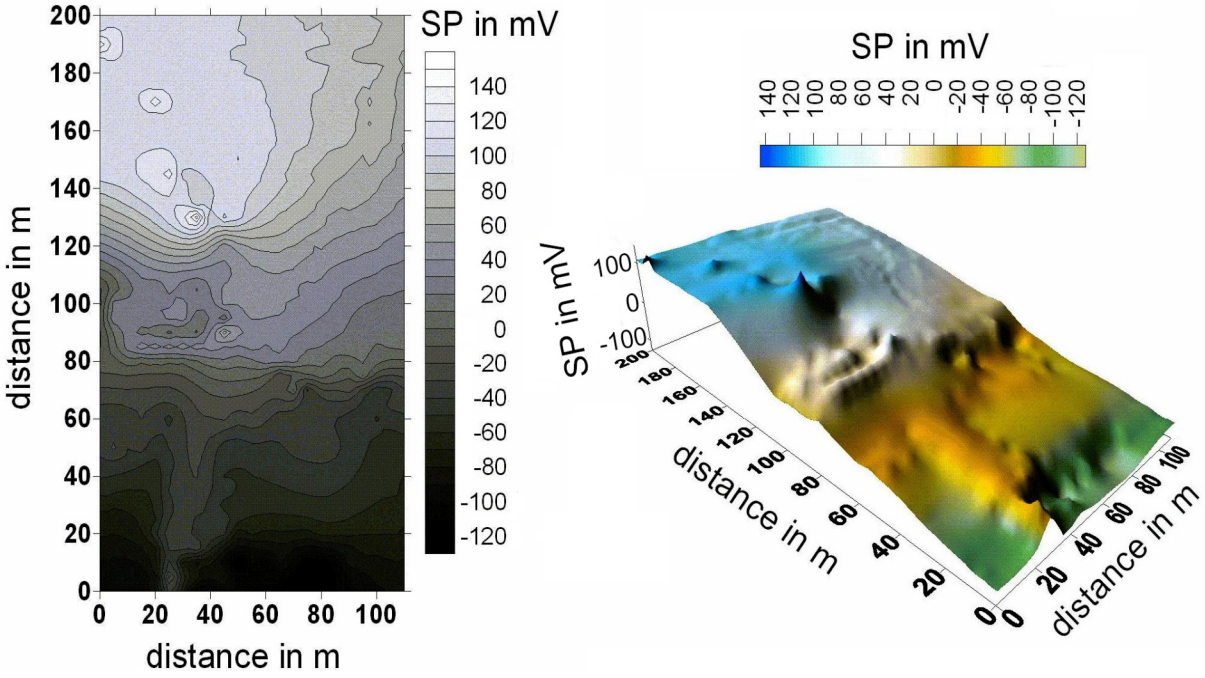

Fig. (9). Example of application of the probability tomography method to a self-potential field dataset collected over a landslide [18]. The self-potential map in the classical 2D base-view (left) and in the equivalent 3D surface-view (right). Note that the slope trend in the right-hand surface-view is strictly determined by the self-potential low wavenumber decrease from the positive to the negative values, as indicated by the vertical axis and the equivalent color scale. It is nearly opposite to the landslide sloping morphology, in the sense that the negative self-potential values appear on the most elevated portion of the surveyed landslide body, while the positive ones occur at the bottom.

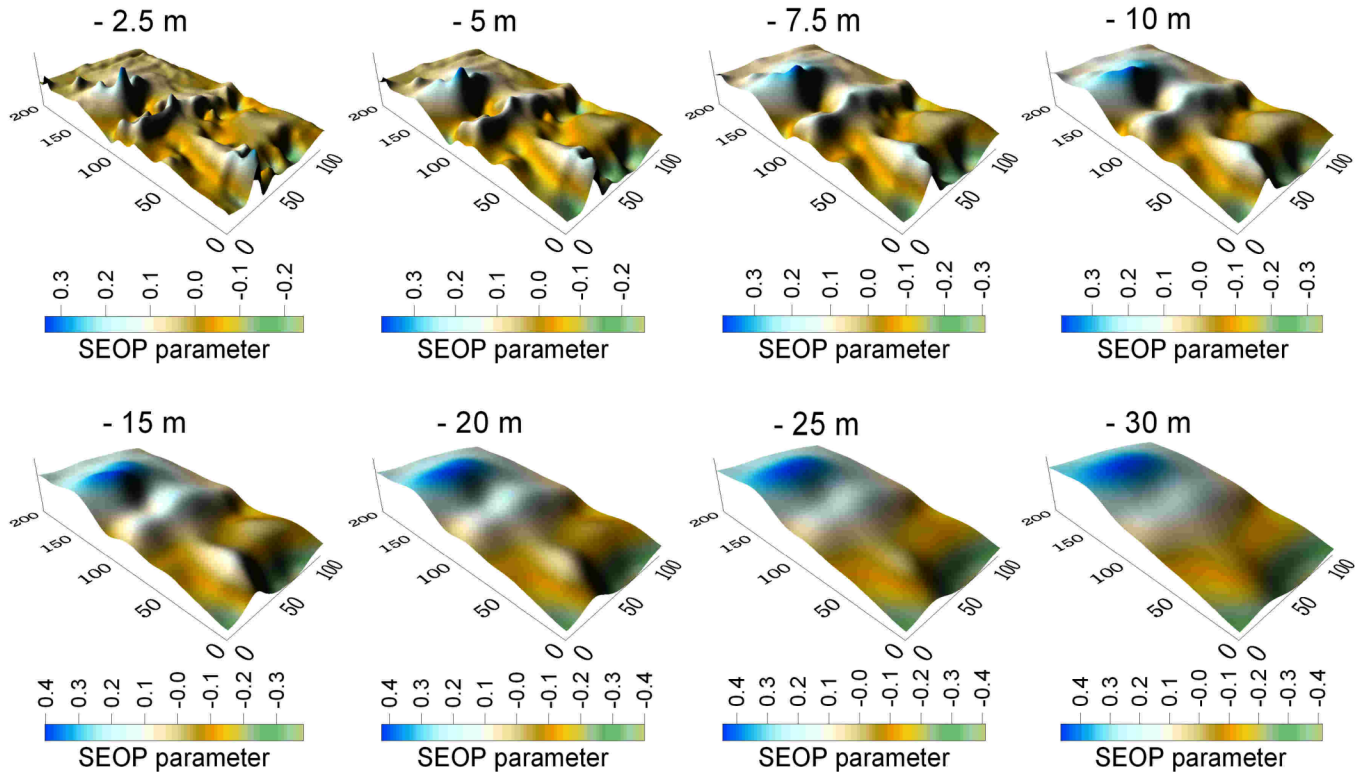

Fig. (10). A set of 3D surface-views of the behavior of the electrical charge occurrence probability function (the SEOP function for the self-potential method) at different depths below ground level, obtained from the map reported in Fig. (**9**) [18]. The depth is shown at the top of each 3D surface plot. In all of the 3D images the vertical axis represent now the SEOP axis, equivalent to the corresponding color scale.

Besides the different physical principles and analytical developments between the two tomography approaches, the most remarkable difference is that the DT method is really a full inversion approach, whereas the PT method is typically a positional imaging approach. In fact, the DT method results in delineating location and shape of the targets as well as estimating the constitutive physical parameters that characterize the target in contrast with the background. A necessary condition for the DT method to be operative is the availability of a priori information. This aspect may become a serious limitation especially when dealing with datasets collected over complex structures, since the risk of a false interpretation rapidly increases if a priori constraints are not suitably selected, or, even worse, if they are imposed with some degree of arbitrariness.

The PT method, instead, aims at highlighting the most probable position and shape of the anomaly source bodies, without the possibility to estimate the constitutive physical parameters. In near-surface geophysics, this has only rarely been considered a serious limitation, as in many target-oriented applications the determination of the intrinsic physical parameter of the source bodies is not so important as the knowledge of the position and shape. Many datasets have been successfully interpreted on this semi-quantitative basis, e.g. in archaeological prospection [19,20]. In all of the cases in which the correct estimate of the true physical parameter is considered essential for assessing the inner properties of the target, the PT results can be used as robust and confident geometric constraints in any of the standard inversion routines.

REFERENCES

[1] D. Patella, "Geophysical tomography in engineering geology: an overview", in Seventh International Congress of the Brazilian Geophysical Society, 2001. Available from: arXiv:physics/0512154v1.

[2] L. R. Lines, and S. Treitel, "Tutorial. A review of least-squares inversion and its application to geophysical problems", *Geophys. Prospect.*, vol. 32, pp. 159-186, Apr 1984.

[3] G. Nolet, "Waveform tomography," in *Seismic Tomography,* G. Nolet, Ed. Dordrecht: Reidel, 1987, pp. 301-322.

[4] K. T. Kilty, and A. L. Lange, "Acoustic tomography in shallow geophysical exploration using a transform reconstruction," in *Geotechnical and Environmental Geophysics,* Vol. III, *Geotechnical,* S. H. Ward, Ed. Tulsa: Society of Exploration geophysicists, 1990, pp. 23-36.

[5] P. Carrion, "Dual tomography for imaging complex structures", *Geophysics*, vol. 56, pp. 1395-1404, Sep 1991.

[6] P. Carrion, J. Costa, J. E. F. Pinheiros, and M. Schoenberg, "Short Note. Cross-borehole tomography in anisotropic media", *Geophysics*, vol. 57, pp. 1194-1198, Sep 1992.

[7] J. G. Berryman, "Lecture notes on nonlinear inversion and tomography: 1. Borehole seismic tomography", revised and expanded Oct 1991. Available from: http://sepwww.stanford.edu/sep/berryman/NOTES/lecture_notes.pdf

[8] D. Patella, "Introduction to ground surface self-potential tomography", *Geophys. Prospect.*, vol. 45, pp. 653-681, Jul 1997.

[9] D. Patella, "Self-potential global tomography including topographic effects", *Geophys. Prospect.*, vol. 45, pp. 843-863, Sep 1997.

[10] P. Mauriello, and D. Patella, "Resistivity anomaly imaging by probability tomography", *Geophys. Prospect.*, vol. 47, pp. 411-429, May 1999.

[11] P. Mauriello, and D. Patella, "Principles of probability tomography for natural-source electromagnetic induction fields", *Geophysics*, vol. 64, pp. 1403-1417, Sep 1999.

[12] P. Mauriello, and D. Patella, "Gravity probability tomography: a new tool for buried mass distribution imaging", *Geophys. Prospect.*, vol. 49, pp. 1-12, Jan 2000.

[13] D. M. McCann, M. Eddleston, P. J. Fenning, and G. M. Reeves, Eds., *Modern Geophysics in Engineering Geology*. London: The Geological Society, 1997.

[14] L. Lines, "Cross-borehole geophysics in the petroleum industry", *Leading Edge*, vol. 12, p. 12, Jan 1993.

[15] D. A. Hollema, and L. D. Olson, "Crosshole sonic logging and velocity tomography imaging of drilled shaft foundations", in Sixth International Symposium on Non-Destructive Testing in Civil Engineering 2003. Available from: http://www.ndt.net/article/ndtce03/papers/v024/v024.htm

[16] G. Buselli, C. Barber, G. B. Davis, and R. B. Salama, "Detection of groundwater contamination near waste disposal sites with transient electromagnetic and electric methods," in *Geotechnical and Environmental Geophysics,* vol. II, *Environmental and Groundwater,* S. H. Ward, Ed. Tulsa: Society of Exploration geophysicists, 1990, pp. 27-40.

[17] J. Zlotnicki, and Y. Nishida, "Review on morphological insights of self-potential anomalies on volcanoes", *Surv. Geophys.*, vol. 24, pp. 291-338, Jul 2003.

[18] S. M. Patella, "Applicazione del metodo geofisico dei potenziali spontanei lungo un versante in frana per lo studio dei flussi idrici sotterranei", Applied Geophysics and Geotechnics Training Course thesis, University Roma Tre, Rome, Italy, 2007.

[19] R. Alaia, D. Patella, and P. Mauriello, "Application of geoelectrical 3D probability tomography in a test-site of the archaeological park of Pompei (Naples, Italy)", *J. Geophys. Eng.*, vol. 5, pp. 67-76, March 2008.

[20] V. Compare, M. Cozzolino, P. Mauriello, and D. Patella, "Three-dimensional resistivity probability tomography at the prehistoric site of Grotta Reali (Molise, Italy)", *Archaeol. Prospect.*, vol. 16, pp. 53-63, Jan 2009.

Received: March 2, 2009 Revised: March 24, 2009 Accepted: March 29, 2009